Acta Pharmaceutica Sinica B 2025;15(8):4030−4046

Chinese Pharmaceutical Association
Institute of Materia Medica, Chinese Academy of Medical Sciences

Acta Pharmaceutica Sinica B

www.elsevier.com/locate/apsb
www.sciencedirect.com

ORIGINAL ARTICLE

Targeted inhibition of macrophage STING signaling alleviates inflammatory injury and ventricular remodeling in acute myocardial infarction

Huan Yao[a,b,†], Qingman He[c,†], Shujun Wei[d,e], Li Xiang[c], Yuanyuan Luo[c], Cong Huang[f], Weiwei Liu[f], Chuan Zheng[b,g,*], Xueping Li[c,*], Yongxiang Gao[c,*]

[a]*Sichuan Provincial Engineering Research Center of Innovative Re-Development of Famous Classical Formulas, Tianfu TCM Innovation Harbour, Chengdu University of Traditional Chinese Medicine, Chengdu 611930, China*
[b]*Sichuan Provincial Engineering Technology Research Center of Natural Small Molecule Drug, Tianfu TCM Innovation Harbour, Chengdu University of Traditional Chinese Medicine, Chengdu 611930, China*
[c]*Hospital of Chengdu University of Traditional Chinese Medicine, Chengdu 610072, China*
[d]*Chengdu University of Traditional Chinese Medicine, Chengdu 611137, China*
[e]*Sichuan Police College, Luzhou 646000, China*
[f]*School of Basic Medical Sciences, Chengdu University of Traditional Chinese Medicine, Chengdu 611137, China*
[g]*TCM Regulating Metabolic Diseases Key Laboratory of Sichuan Province, Hospital of Chengdu University of Traditional Chinese Medicine, Chengdu 610072, China*

Received 5 January 2025; received in revised form 4 March 2025; accepted 29 March 2025

KEY WORDS

Acute myocardial infarction;
Mitochondrial DNA;
Macrophage;
STING signaling;
Myocardial inflammation

Abstract Mitochondrial DNA (mtDNA) acts as a damage-associated molecular pattern to activate the stimulator of interferon genes (STING) signaling in macrophages, promoting tissue inflammation. However, its role in acute myocardial infarction (AMI) remains unclear. Macrophage-specific *Sting1* knockout mice were used to validate STING's pathological role in AMI. Cardiac and liver mtDNA were used to activate macrophages in co-culture systems with cardiomyocytes to assess fibrosis and hypertrophy. Panaxatriol saponin (PTS) was tested for its ability to block mtDNA-driven macrophage activation and subsequent cardiomyocyte damage. STING−PTS binding ability was analyzed. AMI rats received PTS to evaluate its effects on myocardial inflammation and ventricular remodeling. *In vivo*,

*Corresponding authors.
E-mail addresses: zhengchuan@cdutcm.edu.cn (Chuan Zheng), lixueping@cdutcm.edu.cn (Xueping Li), drgaoyx@cdutcm.edu.cn (Yongxiang Gao).
[†]These authors made equal contributions to this work.
Peer review under the responsibility of Chinese Pharmaceutical Association and Institute of Materia Medica, Chinese Academy of Medical Sciences.

https://doi.org/10.1016/j.apsb.2025.06.014

macrophage-specific *Sting1* knockout reduced myocardial inflammation and injury after AMI. *In vitro*, mtDNA-activated macrophages induced cardiomyocyte fibrosis and hypertrophy through STING signaling. PTS suppressed mtDNA-driven macrophage activation by directly binding STING, thereby blocking inflammatory cascades. In AMI rats, PTS treatment attenuated acute inflammation and reversed ventricular remodeling. These findings establish the mtDNA−STING axis in macrophages as a critical driver of post-AMI inflammation and identify pharmacological STING inhibition with PTS as a promising therapeutic strategy. The study bridges genetic validation with translational applications, highlighting macrophage STING as a novel target for ischemic heart disease management.

1. Introduction

Acute myocardial infarction (AMI) and the subsequent development of heart failure are major contributors to global mortality and disability. Despite advancements, the rates of death and illness following AMI remain high, with a 7% mortality rate and 22% of patients dying within 1 year[1]. New treatments are urgently needed to reduce infarction size, prevent adverse left ventricular remodeling, and improve patient outcomes after AMI. The body's inflammatory response to AMI plays a crucial role in determining the extent of the infarction and the subsequent negative remodeling of the left ventricle, highlighting this inflammatory response as a potential therapeutic target to improve clinical outcomes for patients with AMI[2].

The onset of acute myocardial ischemia triggers an early inflammatory response aimed at clearing dead cell debris from the affected region. This initial proinflammatory phase is followed by an anti-inflammatory repair phase, which promotes wound healing and scar formation, thereby preventing cardiac rupture. The regulation of these two phases is delicate and complex, involving both the heart's parenchymal cells and immune cells. Excessive inflammation during the proinflammatory stage exacerbates acute heart damage and leads to unfavorable left ventricular remodeling after AMI[3-5].

In AMI, it is widely believed that the inflammatory response may be partially initiated by damage-associated molecular patterns (DAMPs) such as adenosine triphosphate, mitochondrial DNA (mtDNA), and RNA, which are released from dead and damaged heart cells. These DAMPs act as ligands for pattern-recognition receptors (PRRs), leading to the release of various proinflammatory mediators[6,7]. This process attracts inflammatory cells to the infarcted region of the heart, intensifying the inflammatory response. Furthermore, inflammation extends to the border area of the infarct, where infiltrating white blood cells can damage or kill cardiomyocytes; this worsens ischemic injury beyond the initial myocardial infarct region.

Previous studies have elucidated the mechanisms and therapeutic strategies targeting mtDNA activation of Toll-like receptor 9 (TLR9)-mediated myocardial inflammation[8]. TLR9 activation triggers the nuclear factor kappa B (NF-κB) and NOD-like receptor pyrin domain-containing protein 3 (NLRP3) inflammasome pathways, resulting in elevated levels of inflammatory cytokines such as interleukin (IL)-1β and IL-6, which play critical roles in the progression of heart failure[9-13]. Consequently, the pathways through which mtDNA induces inflammation could serve as potential treatment targets for AMI and heart failure. Certain PRRs that sense mtDNA, including TLR9, Z-DNA binding protein 1, cyclic guanosine monophosphate−adenosine monophosphate (cGAMP) synthase (cGAS), and NLRP3, have been identified to date. Previous studies have elucidated the mechanisms and therapeutic strategies aimed at mitigating myocardial inflammation triggered by the activation of TLR9[8]. More recently, the pivotal role of Z-DNA binding protein 1 in myocardial inflammation and cardiac remodeling has also been highlighted in literature[14]. Regarding NLRP3, it is generally reported that oxidized mtDNA can interact with this receptor[15].

cGAS detects misplaced genomic, mitochondrial, and microbial double-stranded DNA, producing 2′,3′-cGAMP, which activates stimulators of interferon genes (STING) and triggers innate immune responses. This process forms a broad and effective defense mechanism against tissue damage and pathogen invasion[16]. Previous research has highlighted the significant role of the mtDNA-activated cGAS/STING pathway in the context of myocardial injury. For instance, dysregulated mtDNA synthesis within macrophages has been shown to worsen myocardial inflammation and atherosclerosis[17]. Additionally, gasdermin-E-mediated pyroptosis has been identified as a driver of immune checkpoint inhibitor-associated myocarditis, facilitated by the activation of the cGAS−STING pathway[18]. Most notably, mtDNA released from the cytoplasmic lysate can trigger tissue damage through the cGAS−STING pathway, contributing to cardiac dysfunction following pressure overload or doxorubicin exposure[19-21]. Nevertheless, the specific role of macrophage mtDNA-induced STING signaling in the inflammatory response during AMI is still not well understood.

Panaxatriol saponin (PTS), a key active ingredient in *Panax notoginseng*, primarily consists of ginsenoside Rg1, ginsenoside Re, and notoginsenoside R1. It has been used in Chinese clinical practice to treat brain disorders because of its antioxidant, antiplatelet, and angiogenesis-enhancing properties[22-24]. Additionally, previous studies demonstrated the beneficial effects of PTS in myocardial ischemic diseases, including ischemia−reperfusion injury and myocardial fibrosis[25,26]. Crucially, PTS, along with ginsenoside Rg1, ginsenoside Re, and notoginsenoside R1, has been documented to possess significant anti-inflammatory properties[27-30]. Thus, further investigation into the anti-inflammatory effects of PTS in AMI is warranted.

2. Materials and methods

2.1. Reagent

PTS was obtained from Huasun Group Co., Ltd. (Chengdu, China). The key components of PTS, including ginsenoside Rg1, ginsenoside Re, and notoginsenoside R1, were sourced from

Chengdu MUST Bio-Technology Co., Ltd. (Chengdu, China); each compound had a purity of at least 95%.

2.2. Animals

Cyagen Biosciences Inc. (Suzhou, China) utilized the CRISPR-Cas9 technique to create *Sting1*$^{fl/fl}$ mice on a C57BL/6 genetic background. Two *loxP* sequences were inserted in *Sting1* intron 5 and downstream of the stop codon, as shown in Fig. 1N. To generate *Sting1*$^{fl/fl}$-LysMCre mice, C57BL/6 mice with lysozyme M (LysM) promoter-driven Cre recombinase (obtained from Cyagen Biosciences Inc.) were bred with *Sting1*$^{fl/fl}$ mice, enabling targeted deletion of *Sting1* in macrophages.

Male Sprague−Dawley rats aged 8−10 weeks and weighing 180−200 g were obtained from the Chengdu Dashuo Experimental Animal Center (Chengdu, China). All experimental procedures were approved by the Bioethics Committee of Chengdu University of Traditional Chinese Medicine (Reference No. 2022-13).

2.3. Establishment of the AMI model

The AMI model was established as previously described[31]. Briefly, mice or rats were anesthetized *via* intraperitoneal injection of 3% sodium pentobarbital. A 7-0 silk suture was used to permanently occlude the left anterior descending branch of the coronary artery. To alleviate postoperative discomfort, intramuscular buprenorphine HCl was administered immediately after surgery. Ischemia was confirmed by an elevated ST segment on the electrocardiogram. Sham-operated control animals underwent the same surgical procedures except for left anterior descending artery occlusion.

2.4. PTS treatment in vivo

Depending on the purpose of the experiment, rats were treated with PTS for varying durations. To assess the impact of PTS on the acute inflammatory phase, rats were administered PTS at a dosage of 25, 50, or 100 mg/kg/day[25]. The AMI model was established after 3 days of continuous prophylactic administration; an additional dose was given on the day of AMI induction. To evaluate efficacy during the chronic fibrosis and heart failure phases, rats received 25, 50, or 100 mg/kg/day for 3 consecutive days before and after the establishment of the AMI model, followed by euthanasia after echocardiography on Day 30 post-infarction (PI).

2.5. Echocardiography

Cardiac function was noninvasively evaluated using M-mode echocardiography as previously described[32]. In brief, rats were sedated with 1% sodium pentobarbital and positioned supine with their forelimbs extended. The chest and anterior thoracic fur were removed, and a conductive gel was applied to the chest. Transthoracic echocardiography was performed using an Acuson Sequoia model 512 system (Siemens Healthineers, Erlangen, Germany) equipped with a 25-MHz linear transducer. The left ventricular internal dimensions during systole and diastole, fractional shortening, and ejection fraction were measured.

2.6. Histological examination

Heart tissues were fixed with 4% paraformaldehyde and embedded in paraffin. 5-micrometer-thick heart sections were prepared for pathological analysis by deparaffinization, rehydration, and staining with hematoxylin and eosin (H&E) and Masson's trichrome, using standard protocols[33]. The samples were dehydrated with ethanol, cleared with xylene, and mounted with Permount Mounting Medium (Baso, Zhuhai, China). Masson's trichrome staining was performed in accordance with the manufacturer's instructions.

2.7. Enzyme-linked immunosorbent assay (ELISA)

Rat tumor necrosis factor (TNF)-α, IL-6, IL-1β, and interferon (IFN)-α ELISA kits were obtained from Elabscience Biotechnology Co., Ltd. (Wuhan, China). ELISA assays were conducted in accordance with the manufacturer's guidelines.

2.8. Quantification of hydrogen peroxide (H_2O_2) and superoxide anion ($O_2^{\cdot -}$) levels

Levels of H_2O_2 and $O_2^{\cdot -}$ were measured using the Hydrogen Peroxide Content Assay Kit and Micro Superoxide Anion Assay Kit from Solarbio (Beijing, China), in accordance with the manufacturer's instructions. Tissue lysates were prepared, and after centrifugation, the supernatant was collected. Specified reagents were sequentially added as detailed in the instructions. After incubation for 5 min at room temperature, absorbance was measured at either 415 nm or 530 nm using a microplate spectrophotometer. Levels of H_2O_2 and $O_2^{\cdot -}$ were determined using formulas provided in the kit instructions.

2.9. Assays for immunofluorescence (IF) and immunohistochemistry (IHC)

Paraffin-embedded heart sections were heated at 65 °C for 1 h, deparaffinized in xylene, rehydrated in ethanol, and subjected to antigen retrieval using a citric acid solution. Fixed cells were permeabilized with 0.5% Triton X-100 for 30 min. To prevent nonspecific binding, samples were incubated with goat serum for 1 h. The sections or cells were then incubated overnight at 4 °C with primary antibodies, followed by incubation with CoraLite 488- or 594-conjugated secondary antibodies for IF or horseradish peroxidase-conjugated secondary antibodies for IHC. The slides or cells were counterstained with 4′,6-diamidino-2-phenylindole and examined under a fluorescence microscope (Olympus, Tokyo, Japan). The antibodies used are listed in Supporting Information Table S1.

2.10. Extraction of bone marrow cells and macrophage differentiation

Bone marrow cells were isolated and differentiated into macrophages, in accordance with previously described methods[34]. In brief, the femora and tibiae were flushed to collect bone marrow cells. The cells were incubated at 37 °C with 5% CO_2 for 36 h. Non-adherent cells were collected and cultured in α-MEM medium (HyClone, Logan, UT, USA) supplemented with 25 ng/mL macrophage colony-stimulating factor (HUABIO, Hangzhou, China), 10% fetal bovine serum (HyClone), and 1% penicillin−streptomycin (HyClone) for 48 h to generate bone marrow-derived macrophages (BMDMs). The purity of the macrophages obtained was characterized by using flow cytometry, in which F4/80 and CD11b double positivity for macrophages was achieved with 99% purity (Supporting Information Fig. S1A and S1B).

2.11. Isolation and culture of neonatal mouse primary cardiomyocytes

Cardiomyocytes were isolated from neonatal mice (48 ± 6 h post-birth) as previously described[35]. Briefly, mice were euthanized by decapitation; their hearts were collected and placed in a culture dish with chilled Hank's balanced salt solution. The hearts were digested using 1% type II collagenase and trypsin (2:1) without ethylenediaminetetraacetic acid. Approximately 10 million cells were plated in 10-cm petri dishes. After 2 h of sedimentation at 37 °C, non-adherent cells were collected, and adherent cells were discarded. Cardiomyocytes were maintained in Dulbecco's modified Eagle's medium (HyClone) supplemented with 10% fetal bovine serum, 100 U/mL penicillin, and 100 μg/mL streptomycin (HyClone), then incubated at 37 °C with 5% CO_2. Bromodeoxyuridine (0.1 mmol/L) was used to inhibit the growth of residual cardiac fibroblasts and endothelial cells.

2.12. mtDNA isolation and transfection

mtDNA was isolated from mouse hearts or livers using the mtDNA Extractor CT Kit (Wako, Osaka, Japan). Lipofectamine™ 3000 (Invitrogen, Burlingame, CA, USA) was used as the transfection agent.

2.13. Plasmids constructs and transient transfection

Plasmids HA-STING, FLAG-TANK binding kinase 1 (TBK1), and FLAG-interferon regulatory factor 3 (IRF3) were obtained from Addgene (Watertown, MA, USA). Transfections were performed using Lipofectamine™ 3000 (Invitrogen), in accordance with the manufacturer's protocol. Briefly, 1 μg of plasmid (plus 1 μL transfection reagent) and 2.5 μL of transfection reagent were separately mixed in 100 μL Opti-MEM (Invitrogen), combined, and incubated at room temperature for 5 min before addition to the cells. The cells were incubated with the liposome−DNA complexes for 24−48 h, then harvested for experiments.

2.14. Knockdown Cgas and overexpression of Sting1

Adenoviruses for *Cgas* knockdown (Ad-sh*Cgas*), wild-type *Sting1* overexpression (Ad-oe*Sting1*, WT), or *Sting1* overexpression with STING protein mutations Tyr261Ala and Thr263Ala (Ad-oe*Sting1*, mutant) were acquired from GeneChem. (Shanghai, China). In short, RAW264.7 or BMDMs were placed in six-well plates at a density of 5×10^5 cells per well and treated with 5 μg/mL polybrene (Beyotime, Haimen, China) along with adenovirus for 4 days to knockdown *Cgas* or overexpression *Sting1*.

2.15. Quantitative real-time polymerase chain reaction (qRT-PCR)

Quantification of cytosolic mtDNA was performed as previously described, with minor modifications[14]. Briefly, the heart tissues were homogenized in a 100 mmol/L Tricine-NaOH buffer (pH 7.4) containing 0.25 mol/L sucrose, 1 mmol/L EDTA, and a protease inhibitor, then centrifuged at 800 × *g* for 15 min at 4 °C. Protein levels and supernatant volumes were equalized; the samples were centrifuged at 120,000 × *g* for 40 min at 4 °C to obtain the cytosolic fraction. DNA was extracted from 200 μL of the cytosolic fraction using the DNeasy Blood & Tissue Kit (Qiagen, Valencia, CA, USA). qRT-PCR was performed to measure DNA copy numbers for *Dloop*, *Tert*, and *B2m*, using equal volumes of the DNA solution. The primer sequences utilized for qRT-PCR were as follows:

Dloop: Forward 5′-GAAATCAACAACCCGCCCAC-3′, Reverse 5′-ACGGCTATGTTGAGGAAGGC-3′;

Tert: Forward 5′-CTACATCACAGAGACCACGTT-3′, Reverse 5′-CCTCTTGTGACAGTTCCCGTA-3′;

B2m: Forward 5′-TGTGCGGTTTTCATCACCCAA-3′, Reverse 5′-GCCCTTCATCGAGCACCT-3′.

2.16. Western blot analysis

Western blotting was performed as described in previous studies[26]. In brief, proteins were extracted from cells or tissues using a radioimmunoprecipitation assay buffer, and their concentrations were determined using the bicinchoninic acid protein assay kit (Beyotime). Proteins were separated on a 10% sodium dodecyl sulfate-polyacrylamide gel electrophoresis gel and transferred to polyvinylidene fluoride membranes. The membranes were blocked with 5% skim milk in Tris-buffered saline for 1 h, then incubated overnight with primary antibodies at 4 °C. Subsequently, the membranes were incubated with horseradish peroxidase-linked secondary antibodies at room temperature for 1 h. After membranes had been washed, protein bands were detected using enhanced chemiluminescence. The antibodies used in this study are listed in Supporting Information Table S1.

2.17. Co-immunoprecipitation (Co-IP)

Co-IP was performed using a Co-IP Kit with Protein A + G Magnetic Beads (Beyotime), in accordance with the manufacturer's protocols. Briefly, antibodies (10 μg) were incubated with magnetic beads (25 μL) for 1 h. The cell extracts were incubated with antibody-bound magnetic beads overnight on a rotating device at 4 °C. Proteins were separated from the magnetic beads and analyzed by Western blotting.

2.18. Transmission electron microscopy

Tissues were trypsinized and fixed with glutaraldehyde. Following treatment with 1% osmium tetroxide and 0.1% potassium ferricyanide, samples were dehydrated with ethanol and embedded in epoxy resin. Ultrathin sections (60−80 nm) were prepared using an ultramicrotome (Leica, Wetzlar, Germany). Sections were stained with 2% uranyl acetate in saturated ethanol and lead citrate, and then imaged using an HT7700 electron microscope (Hitachi, Tokyo, Japan).

2.19. Molecular docking

Molecular docking was performed using AutoDock Vina software. The crystal structure of STING (PDB ID: 4EF4) was obtained from the RCSB Protein Data Bank (http://www.rcsb.org). STING was dehydrated, small-molecule ligands were removed, and the resulting structure was saved in PDB format. The two-dimensional structures of ginsenoside Rg1 (CID: 441923), notoginsenoside R1 (CID: 441934), and ginsenoside Re (CID: 441921) were obtained from PubChem (https://pubchem.ncbi.nlm.nih.gov/). Docking results were evaluated based on predicted binding configurations and binding energies (kcal/mol). PyMOL 2.6 software was used to create three-dimensional visualizations of the interactions between PTS components and STING.

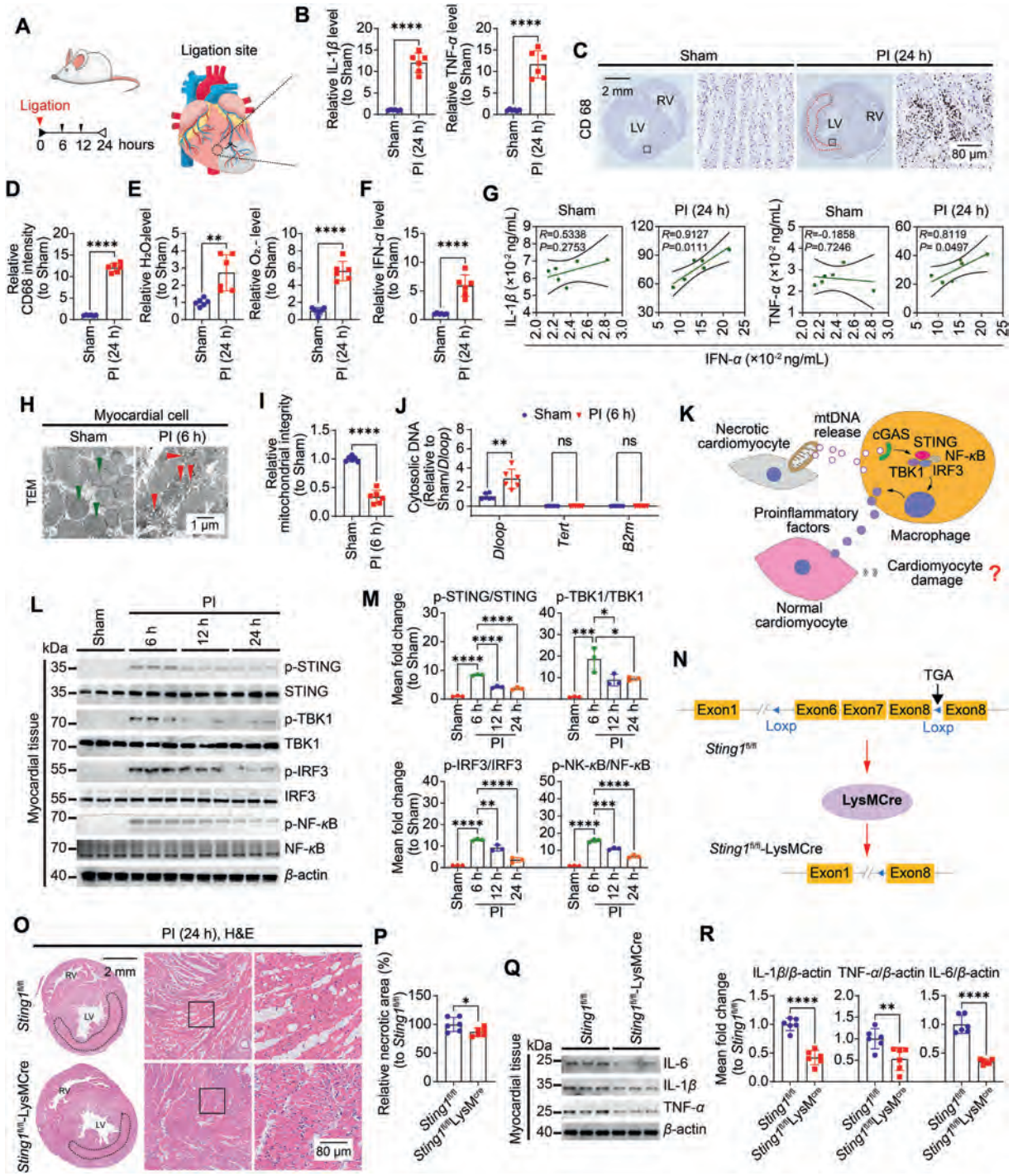

Figure 1 mtDNA-activated macrophages exacerbate myocardial injury in AMI. (A) The schematic illustrates ligation sites and infarction times in an acute myocardial infarction (AMI) model, in which the left anterior descending coronary artery was ligated for 6, 12, or 24 h to induce AMI. (B) Interleukin (IL)-1β and tumor necrosis factor (TNF)-α levels in peri-infarct tissues were analyzed using enzyme-linked immunosorbent assay (ELISA) at 24 h post-infarction (PI) ($n = 6$). (C) Myocardial slices were stained with CD68 antibody 24 h PI; the positive signals were quantified and analyzed in (D) using ImageJ ($n = 6$). (E) Reactive oxygen species (H_2O_2 and $O_2\cdot^-$) in peri-infarct tissues were measured ($n = 6$). (F) Interferon (IFN)-α levels in peri-infarct tissues were assessed using ELISA ($n = 6$). (G) The relationship between IFN-α and IL-1β/TNF-α was analyzed *via* linear regression. (H) Mitochondrial integrity in infarcted myocardium was observed using transmission electron microscopy; quantitative and statistical analyses are presented in (I) ($n = 6$). (J) mtDNA content in peri-infarct myocardial tissues was determined using quantitative reverse transcription polymerase chain reaction (qRT-PCR) 6 h PI ($n = 6$). (K) Schematic showing that mtDNA from necrotic cardiomyocytes activates the macrophage STING inflammatory pathway, exacerbating myocardial injury. (L) Expression patterns of phosphorylated stimulator of interferon genes (p-STING), phosphorylated TANK binding kinase 1 (p-TBK1), phosphorylated interferon regulatory factor 3 (p-IRF3), and phosphorylated nuclear factor kappa B (p-NF-κB) in peri-infarct tissues were detected *via* immunoblotting at 6, 12, and 24 h PI;

2.20. Surface plasmon resonance (SPR)

SPR was conducted as previously described[36]. The binding affinities of ginsenoside Rg1, ginsenoside Re, and notoginsenoside R1 to the STING protein were assessed using the Biacore 1K system (Cytiva, Marlborough, MA, USA). Human recombinant STING protein (MedChemExpress, Shanghai, China) was immobilized on the chip using a standard amine coupling procedure. Sensorgrams were obtained by injecting various concentrations of ginsenoside Rg1, ginsenoside Re, and notoginsenoside R1 (0.1, 0.4, 1.2, 3.7, 11.1, and 33.3 μmol/L) over the immobilized STING surface. The data were processed to determine equilibrium dissociation constant values.

2.21. Cellular thermal shift assay (CETSA)

The CETSA was conducted as previously described following the established protocols for assessing protein−ligand interactions and thermal stability[37]. In brief, cells were incubated with PTS at 37 °C for 2 h, after which they were subjected to 3 min of heating at varying temperatures. Following cooling to room temperature, the cells were harvested and subjected to five cycles of liquid nitrogen freeze−thawing to facilitate lysis. Subsequently, sodium dodecyl sulfate loading buffer was added to the lysates, which were then boiled before being analyzed *via* sodium dodecyl sulfate-polyacrylamide gel and subsequent immunoblotting to assess cGAS or STING expression.

2.22. Statistical analysis

Quantitative data are presented as mean ± standard deviations (SD). The statistical analysis was performed using GraphPad Prism software (version 9.5.1, GraphPad Software, San Diego, CA, USA). For the comparison between two independent groups, an independent sample *t*-test was used. One-way analysis of variance (One-way ANOVA) followed by Tukey's *post hoc* test was used to compare multiple groups. A *P*-value of <0.05 was considered statistically significant.

3. Results

3.1. mtDNA-activated macrophages exacerbate myocardial injury in AMI

Abnormal remodeling of the heart muscle following AMI significantly contributes to heart failure; there is evidence that macrophage-driven inflammation plays a crucial role in regulating heart muscle damage and remodeling shortly after AMI. However, it remains unclear whether macrophage-driven inflammation PI exacerbates damage in the peri-infarct region. To address this issue, we first established a rat model of AMI by ligating the left anterior descending branch of the coronary artery (Fig. 1A). After 24 h of ischemia, significantly elevated levels of IL-1β and TNF-α were observed in the peri-infarct area (Fig. 1B). Because macrophages play a key role in releasing inflammatory mediators after AMI, we examined their distribution in myocardial tissue surrounding the infarct area. IHC staining of myocardial sections using CD68 antibody, a known macrophage marker, revealed substantial accumulation of CD68-positive cells around the infarcted myocardium (Fig. 1C and D) along with a considerable increase in reactive oxygen species (ROS) (Fig. 1E). Further analysis of inflammatory markers in heart tissue revealed a notable increase in IFN-α levels in the peri-infarct area at 24 h PI (Fig. 1F). Notably, the IFN-α levels were correlated with the elevated IL-1β and TNF-α levels (Fig. 1G).

Previous studies have shown that cellular debris from necrotic cells, including mtDNA, can act as DAMPs, triggering immune cell activation. We hypothesized that mtDNA released from lysed mitochondria in damaged heart tissue could activate macrophages in the surrounding area. To test this, we first examined the mitochondrial integrity of cardiomyocytes in the infarcted region. As shown in Fig. 1H and I, mitochondrial integrity was compromised; the membrane rupture was observed in the infarcted heart muscle cells at 6 h PI. We also detected an abundance of *Dloop*, a region of mtDNA, in the cytoplasm of both normal and infarcted hearts, with a substantial increase in *Dloop* levels in the peri-infarct area. In contrast, detectable levels of nuclear DNA components *Tert* and *B2m* were not observed in either the control or peri-infarct myocardial tissues (Fig. 1J). Considering the significant rise in mtDNA in the peri-infarct region and the observed inflammatory response, we hypothesized that dying cardiomyocytes release mtDNA, which activates macrophages in surrounding unaffected myocardium, thereby contributing to post-AMI myocardial damage (Fig. 1K).

It has been reported that cGAS, a protein that detects cytoplasmic DNA, binds to mtDNA and facilitates the movement of STING from the endoplasmic reticulum to the Golgi apparatus. This process activates TBK1, IRF3, and NF-κB, leading to the secretion of type I interferons and various inflammatory cytokines. To determine whether necrotic cardiomyocyte mtDNA activates macrophages *via* this pathway, we assessed the activation status of the STING pathway in the peri-infarct heart tissue. Intriguingly, as shown in Fig. 1L and M, phosphorylated STING (p-STING), phosphorylated TBK1 (p-TBK1), phosphorylated IRF3 (p-IRF3), and phosphorylated NF-κB (p-NF-κB) were substantially increased in the peri-infarct region 6 h after infarction, suggesting that mtDNA from necrotic heart cells triggers the cGAS/STING pathway in the myocardium near the infarcted area. However, it has been unclear whether activation of the macrophage STING pathway contributes to myocardial injury in the peri-infarct myocardium. To investigate this potential contribution, we used CRISPR-Cas9 to specifically knock out the *Sting1* gene in mouse myeloid mononuclear macrophages (Fig. 1N). Remarkably, at 24 h PI, H&E staining results indicated the extent of heart damage was significantly reduced in *Sting1*$^{fl/fl}$-LysMCre mice relative to *Sting1*$^{fl/fl}$ mice (Fig. 1O and P), along with substantial decreases in inflammatory markers such as IL-6, IL-1β, and TNF-α (Fig. 1Q and R).

gray values were quantified and analyzed in (M) using ImageJ ($n = 3$). (N) Schematic representation of specific *Sting1* knockout in the mouse monocyte−macrophage system to construct *Sting1*$^{fl/fl}$-LysMCre mice. These mice were used to induce AMI and were euthanized 24 h PI. (O) Representative hematoxylin and eosin (H&E)-stained images of mouse heart sections. (P) Myocardial injury area was quantified and statistically analyzed using ImageJ ($n = 6$). (Q) IL-6, IL-1β, and TNF-α levels in peri-infarct tissues were determined *via* Western blotting; gray values were quantified in (R) using ImageJ ($n = 6$). Data are presented as mean ± SD. *$P < 0.05$, **$P < 0.01$, ***$P < 0.001$, ****$P < 0.0001$ (ns, no significance). *P* values were calculated based on *t*-test or one-way ANOVA. TEM, transmission electron microscopy.

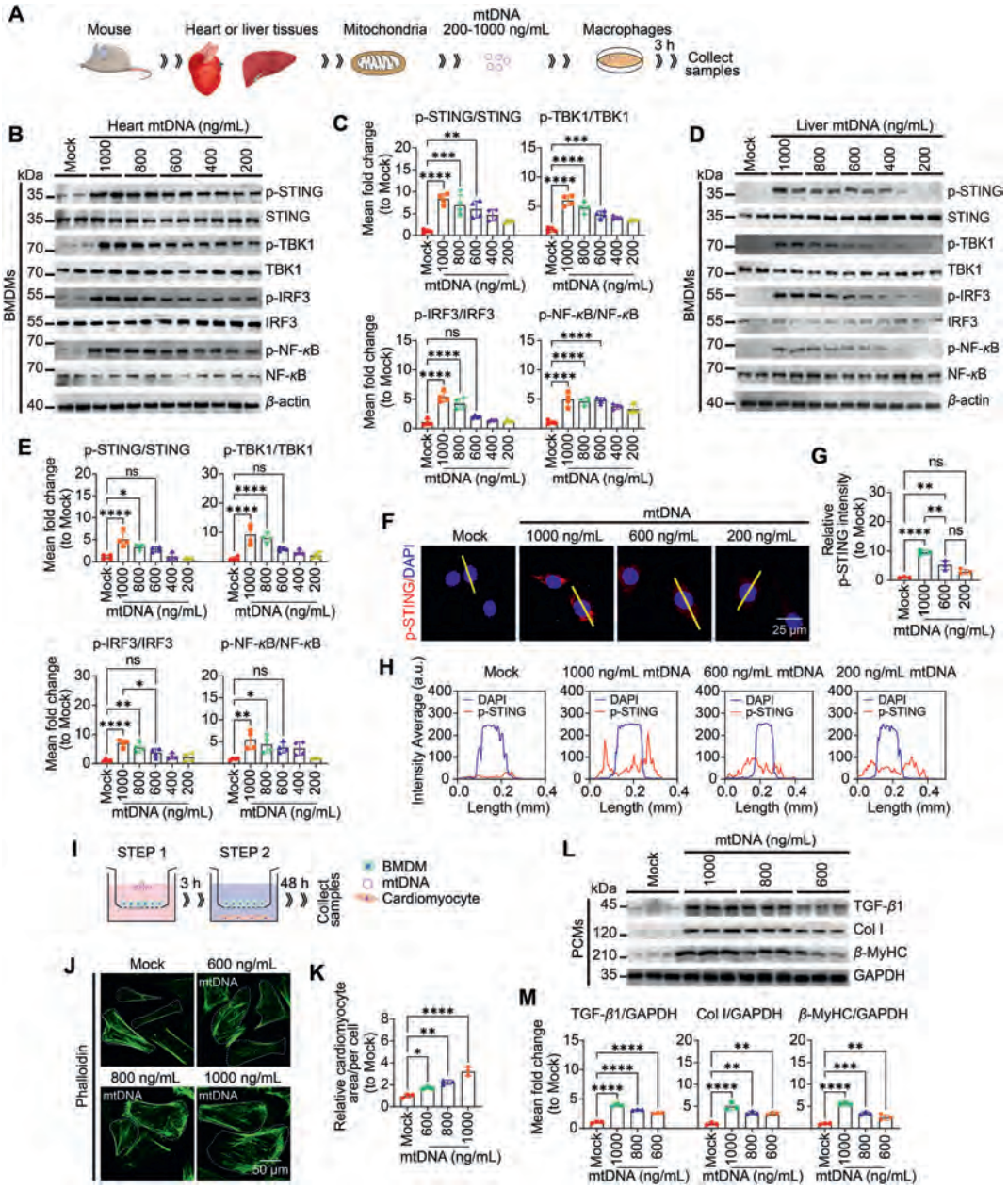

Figure 2 mtDNA-activated macrophages induce cardiomyocyte fibrosis and hypertrophy. (A) The schematic represents mtDNA isolated from mouse heart and liver for macrophage treatment. Bone marrow-derived macrophages (BMDMs) were transfected with 200−1000 ng/mL of cardiac-derived mtDNA, and samples were collected at 3 h post-transfection. (B) p-STING, p-TBK1, p-IRF3, and p-NF-κB levels were measured *via* Western blotting; gray value quantification and analysis were performed in (C) using ImageJ ($n = 4$). (D) BMDMs were transfected with 200−1000 ng/mL of liver-derived mtDNA. The same measurements were conducted as displayed in (B); gray value quantification was performed in (E) using ImageJ ($n = 4$). (F) Representative images of p-STING immunofluorescence (IF) staining in BMDMs. (G, H) Fluorescence intensity of p-STING was assessed using ImageJ ($n = 3$). (I) BMDMs were transfected with 600−1000 ng/mL of liver-derived mtDNA for 3 h, followed by co-culture with primary cardiomyocytes for 48 h. (J) Cardiomyocytes were stained with FITC-conjugated phalloidin; area quantification and analysis were performed in (K) using ImageJ ($n = 3$). (L) Transforming growth factor (TGF)-β1, collagen (Col) I, and β-myosin heavy chain (MyHC) levels were detected *via* Western blotting; gray value quantification and analysis were performed in (M) using ImageJ ($n = 3$). Data are presented as mean ± SD. $^{*}P < 0.05$, $^{**}P < 0.01$, $^{***}P < 0.001$, $^{****}P < 0.0001$ (ns, no significance). *P* values were calculated based on one-way ANOVA. PCMs, primary cardiomyocytes.

3.2. mtDNA-activated macrophages induce cardiomyocyte fibrosis and hypertrophy

Next, we explored whether mtDNA-triggered macrophage activation contributed to cardiomyocyte damage. As shown in Fig. 2A, we extracted mtDNA from the hearts or livers of mice and introduced it into mouse BMDMs. Cardiac mtDNA at concentrations of 800−1000 ng/mL significantly induced the phosphorylation of STING, TBK1, IRF3, and NF-κB in macrophages (Fig. 2B and C). Similarly, we introduced mouse liver mtDNA

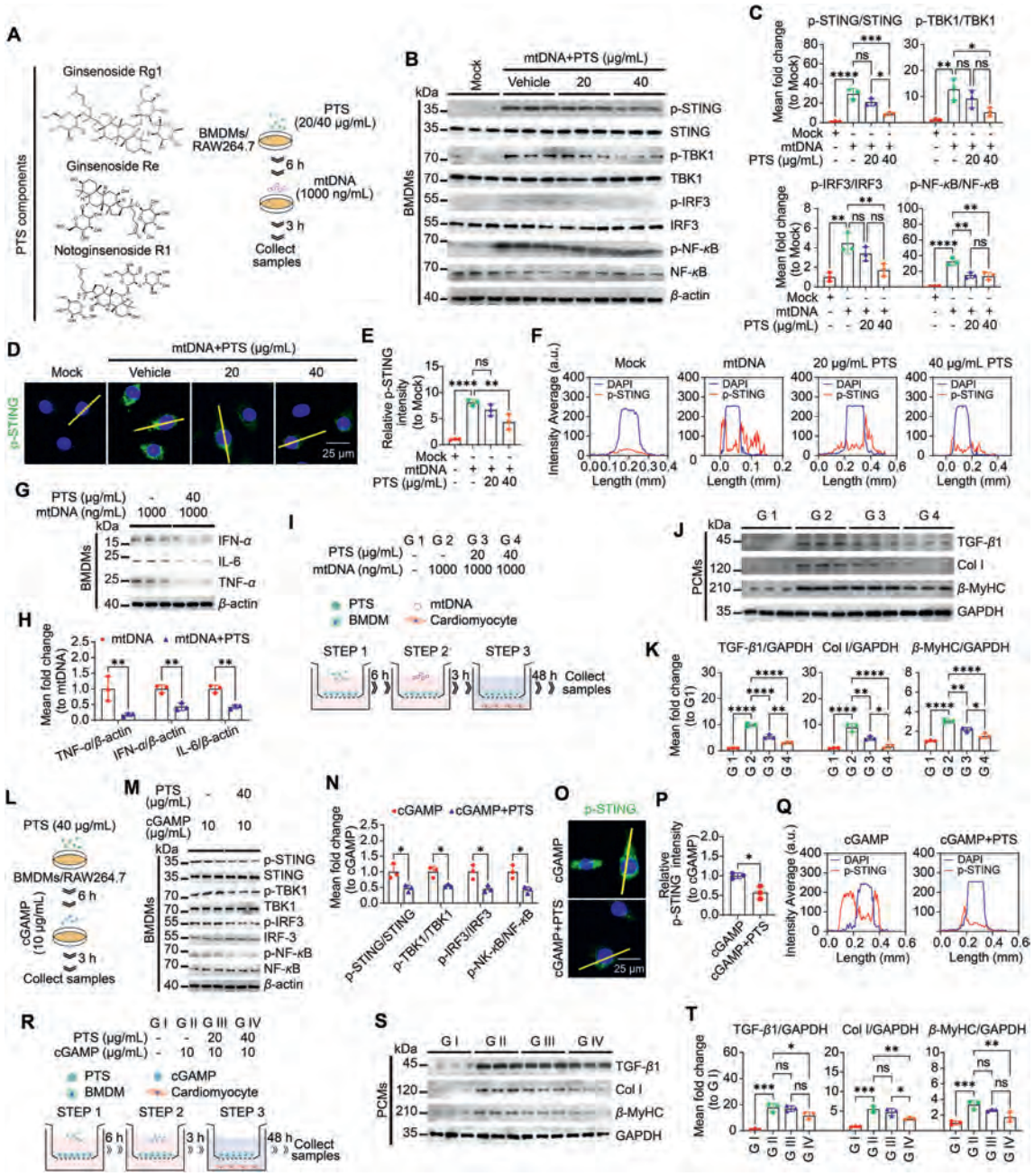

Figure 3 PTS attenuates mtDNA-induced macrophage activation. (A) The schematic shows panaxatriol saponin (PTS) components and cell processing, where BMDMs or RAW264.7 cells were pretreated with 20 or 40 μg/mL of PTS for 6 h, followed by transfection with 1000 ng/mL of mtDNA for 3 h. (B) p-STING, p-TBK1, p-IRF3, and p-NF-κB levels were measured *via* Western blotting; gray value quantification and analysis were performed in (C) using ImageJ ($n = 3$). (D) Representative p-STING IF images; fluorescence intensity quantification was conducted in (E, F) using ImageJ ($n = 3$). (G) BMDMs were pretreated with 40 μg/mL of PTS for 6 h, followed by transfection with 1000 ng/mL of mtDNA for 48 h. IFN-α, IL-6 and TNF-α levels were measured *via* Western blotting; gray value quantification and analysis were performed in (H) using ImageJ ($n = 3$). (I) BMDMs were pretreated with 20 or 40 μg/mL of PTS for 6 h, followed by transfection with 1000 ng/mL of mtDNA for 3 h, and then co-cultured with cardiomyocytes for 48 h. (J) TGF-β1, Col I, and β-MyHC levels were assayed *via* Western blotting; gray value quantification was performed in (K) using ImageJ ($n = 3$). (L) BMDMs or RAW264.7 cells were pretreated with 40 μg/mL of PTS for 6 h, then treated with 10 μg/mL of cGAMP disodium salt for 3 h. (M) p-STING, p-TBK1, p-IRF3, and p-NF-κB levels were measured *via* Western blotting; gray value quantification was conducted in (N) using ImageJ ($n = 3$). (O) Representative IF images of p-STING; fluorescence intensity quantification was carried out in (P, Q) using ImageJ ($n = 3$). (R) BMDMs were pretreated with PTS for 6 h, followed by treatment with 10 μg/mL of cGAMP disodium salt for 3 h, and then co-cultured with cardiomyocytes for 48 h. (S) TGF-β1, Col I, and β-MyHC levels were assayed *via* Western blotting; gray value quantification was performed in (T) using ImageJ ($n = 3$). Data are presented as mean ± SD. $^*P < 0.05$, $^{**}P < 0.01$, $^{***}P < 0.001$, $^{****}P < 0.0001$ (ns, no significance). *P* values were calculated based on *t*-test or one-way ANOVA.

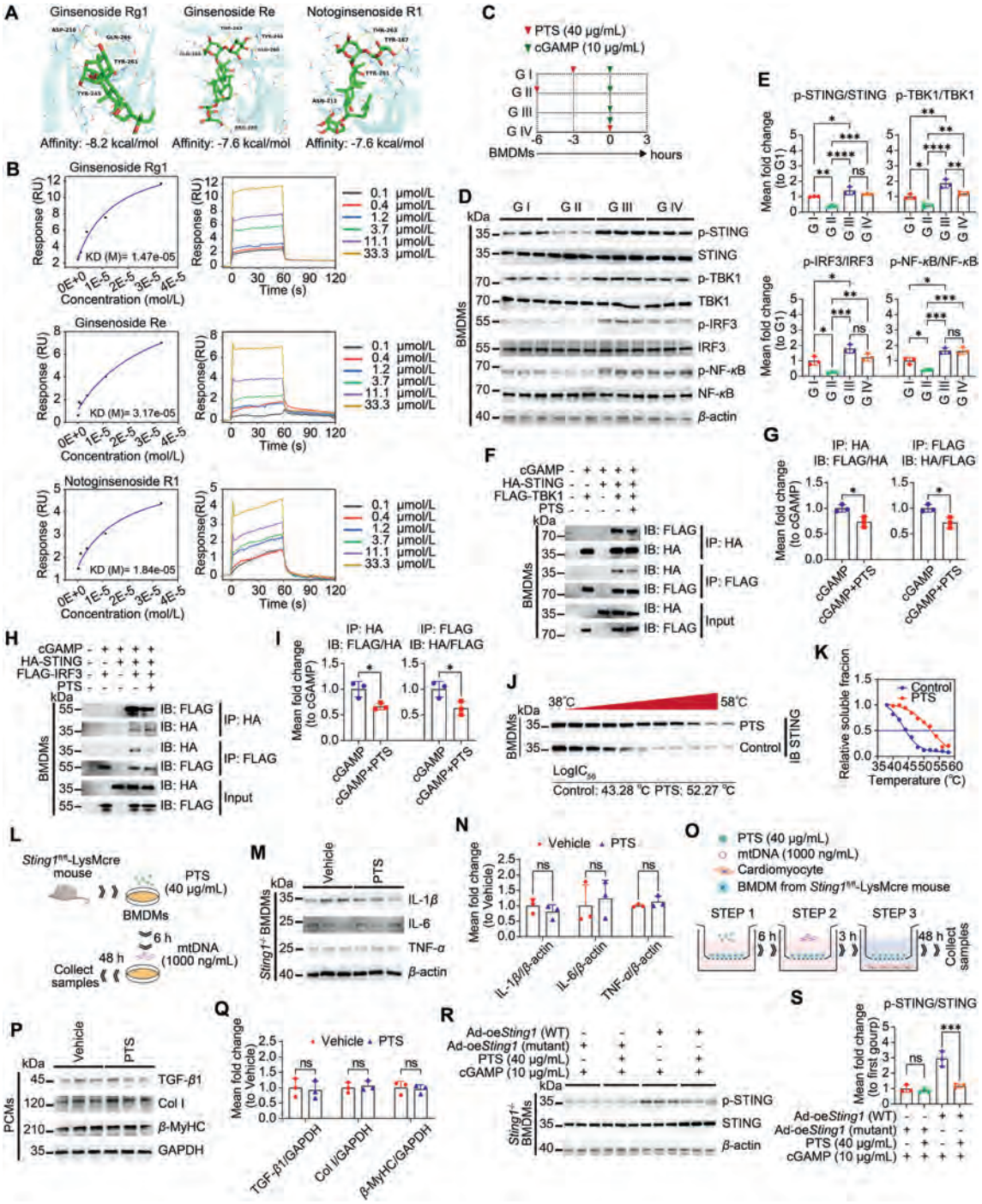

Figure 4 PTS binding to STING inhibits inflammatory signaling in macrophages. (A) Molecular docking results for ginsenoside Rg1, ginsenoside Re, and notoginsenoside R1 with STING. (B) The abilities of PTS to bind STING were examined using surface plasmon resonance. (C) BMDMs, isolated from normal mice, were pretreated with PTS for 6, 3, or 0 h, then treated with cGAMP disodium salt for 3 h. (D) p-STING, p-TBK1, p-IRF3, and p-NF-κB levels were detected *via* Western blotting; gray value quantification was performed in (E) using ImageJ ($n = 3$). BMDMs transfected with HA-STING, FLAG-TBK1, or FLAG-IRF3 plasmid for 48 h were treated with 40 μg/mL of PTS for 6 h, followed by treatment with 10 μg/mL of cGAMP disodium salt for 3 h. (F) The binding abilities of STING and TBK1 were detected *via* co-immunoprecipitation; gray value quantification was conducted in (G) using ImageJ ($n = 3$). (H) The binding abilities of STING and IRF3 were similarly detected; gray value quantification was carried out in (I) using ImageJ ($n = 3$). (J) The interaction of PTS with STING was detected using cellular thermal shift assay and the proteolytic thermolysis curves were plotted in (K). (L) BMDMs isolated from *Sting1*$^{fl/fl}$-LysMCre mice were pretreated with 40 μg/mL of PTS for 6 h, followed by intervention with mtDNA (1000 ng/mL) for 48 h. (M) IL-1β, IL-6, and TNF-α levels were detected *via* Western blotting; gray value quantification was performed in (N) using ImageJ ($n = 3$). (O) BMDMs, isolated from *Sting1*$^{fl/fl}$-LysMCre mice, were pretreated with 40 μg/mL of PTS for 6 h, followed by intervention with mtDNA (1000 ng/mL) for 3 h. These BMDMs were then co-cultured with cardiomyocytes for 48 h. (P, Q) TGF-β1, Col I, and β-MyHC levels were detected and quantified using

into BMDMs. Both Western blot and IF analyses showed that mtDNA at concentrations of 800−1000 ng/mL activated the STING pathway in these cells (Fig. 2D−H). Considering the higher abundance of mtDNA in the liver, we used mouse liver mtDNA to induce macrophage activation in subsequent studies. Cardiomyocyte enlargement due to ventricular remodeling PI is a major contributor to heart failure. To investigate the impact of mtDNA-triggered macrophage activation on this hypertrophy, we transfected macrophages with mtDNA for 3 h and then co-cultured them with primary mouse cardiomyocytes (Fig. 2I). Unexpectedly, after 48 h of co-culture with mtDNA-activated macrophages (600, 800, or 1000 ng/mL), cardiomyocytes exhibited significant hypertrophy (Fig. 2J and K). Subsequent immunoblotting indicated that mtDNA-stimulated macrophages enhanced the levels of transforming growth factor (TGF)-β1 (a pro-fibrotic factor), collagen type I (Col I), and β-myosin heavy chain (MyHC, a marker of cardiac hypertrophy) in cardiomyocytes (Fig. 2L and M). These findings suggest that macrophages activated by mtDNA after myocardial infarction mediate myocardial inflammation and cardiomyocyte injury.

3.3. *PTS attenuates mtDNA-induced macrophage activation*

Our previous studies demonstrated that PTS could attenuate myocardial fibrosis and partially reverse ventricular remodeling[25]. Although PTS has been reported to reduce myocardial inflammation, its effects on mtDNA-mediated macrophage inflammatory responses in AMI remain largely unknown. We thus first pretreated mouse BMDMs with 20 or 40 μg/mL of PTS for 6 h, followed by transfection with 1000 ng/mL of mtDNA for 3 h (Fig. 3A). Western blot and IF analysis indicated that pre-exposure to 40 μg/mL of PTS for 6 h significantly reduced the phosphorylation of STING, TBK1, IRF3, and NF-κB (Fig. 3B−F). Furthermore, we conducted *in vitro* assessments of IFN-α, a downstream effector of IRF3, and IL-6 and TNF-α, which are downstream inflammatory mediators of NF-κB, to evaluate the impact of PTS on these different pathways. The Western blot results reveal that PTS also diminishes the expression of these proteins, thereby underscoring the inhibitory influence of PTS on both the IRF3 and NF-κB signaling pathways (Fig. 3G and H). We also conducted experiments with the mouse monocyte-macrophage cell line RAW264.7, which showed similar results; PTS pretreatment considerably reduced the phosphorylation levels of STING, TBK1, IRF3, and NF-κB (Supporting Information Fig. S2A and S2B). Next, we pretreated BMDMs with 20 or 40 μg/mL of PTS for 6 h before transfecting the cells with mtDNA for 3 h, followed by co-culture with cardiomyocytes (Fig. 3I). Intriguingly, as demonstrated by the immunoblotting results, PTS pretreatment reversed the hypertrophic and fibrotic phenotypes in co-cultured cardiomyocytes (Fig. 3J and K). To further validate the effect of PTS on macrophage STING signaling, we directly used cGAMP, a STING agonist, instead of mtDNA (Fig. 3L). Considering that 40 μg/mL of PTS had a stronger inhibitory effect, we used this concentration to pretreat BMDMs or RAW264.7 cells. Western blot analysis confirmed that pre-exposure to 40 μg/mL of PTS for 6 h substantially decreased the phosphorylation levels of STING, TBK1, IRF3, and NF-κB in both BMDMs and RAW264.7 cells (Fig. 3M and N, Fig. S2C and S2D). IF data similarly showed that PTS reduced cGAMP-induced p-STING expression in BMDMs (Fig. 3O−Q). When we co-cultured PTS and cGAMP-treated BMDMs with cardiomyocytes (Fig. 3R), the data showed that PTS pretreatment reversed the hypertrophic and fibrotic phenotypes of cardiomyocytes (Fig. 3S and T).

Acknowledging the distinct roles that various macrophage subtypes play in inflammatory processes, both pro-inflammatory and anti-inflammatory, we delved into the differential regulatory influences of PTS on the STING pathway within M1 and M2 macrophages. We induced the differentiation of BMDMs into M1-type macrophages with lipopolysaccharide and IFN-γ, or M2-type macrophages with IL-4. Post-differentiation, we investigated the modulatory impact of PTS on the cGAMP-induced activation of the STING pathway in both M1 and M2 macrophages. The results, as depicted in Supporting Information Fig. S3A−S3D, revealed that PTS selectively dampened the activation of the STING signaling pathway in M1-type macrophages, with no significant effect observed in M2-type macrophages. We also elected to investigate the direct effects of PTS on STING activation in cardiomyocytes. Western blot analysis revealed that PTS did not influence the activation of p-STING in cardiomyocytes stimulated with cGAMP (Supporting Information Fig. S4A and S4B), suggesting that PTS may not directly engage in the STING-mediated immune response within cardiomyocytes.

3.4. *PTS binding to STING inhibits inflammatory signaling in macrophages*

The above analysis suggested that PTS has a regulatory effect on the macrophage STING pathway. We therefore investigated the underlying mechanisms. First, we examined the direct effect of PTS on cGAS expression, the mtDNA receptor, but we found no significant effect (Supporting Information Fig. S5A and S5B). Next, we downregulated the cGAS expression in RAW264.7 cells and investigated the impact of PTS on the activation of the STING pathway within these cGAS-knockdown macrophages. The results presented in Fig. S5C and S5D reveal that PTS treatment continued to suppress the activation of the STING pathway in the cGAS knockdown cells, as compared to the control group. In addition, CETSA assay results indicated that PTS treatment did not significantly protect cGAS from temperature-induced proteolysis (Fig. S5E and S5F). Cumulatively, these findings imply that cGAS may not serve as a viable target for PTS-mediated intervention within the STING signaling pathway.

The above data led us to explore whether PTS directly binds to STING to regulate its phosphorylation and downstream signaling. Molecular docking analysis revealed that PTS components, including ginsenoside Rg1, ginsenoside Re, and notoginsenoside R1, exhibit binding affinities of −8.2, −7.6, and −7.6 kcal/mol, respectively, with STING. The interaction sites included ASP-210, GLN-266, TYR-261, TYR-245, THR-263, TYR-240, GLU-260,

ImageJ ($n = 3$). (R) Adenovirus vectors were used to achieve overexpression of the wild-type *Sting1* or a *Sting1* variants in BMDMs isolated from *Sting1*$^{fl/fl}$-LysMCre mice. Following adenovirus infection, BMDMs were pretreated with PTS (40 μg/mL) for 6 h, then treated with 10 μg/mL of cGAMP disodium salt for 3 h. The expression of p-STING was detected *via* Western blotting; gray value quantification was performed in (S) using ImageJ ($n = 3$). Data are presented as mean ± SD. *$P < 0.05$, **$P < 0.01$, ***$P < 0.001$, ****$P < 0.0001$ (ns, no significance). *P* values were calculated based on *t*-test or one-way ANOVA.

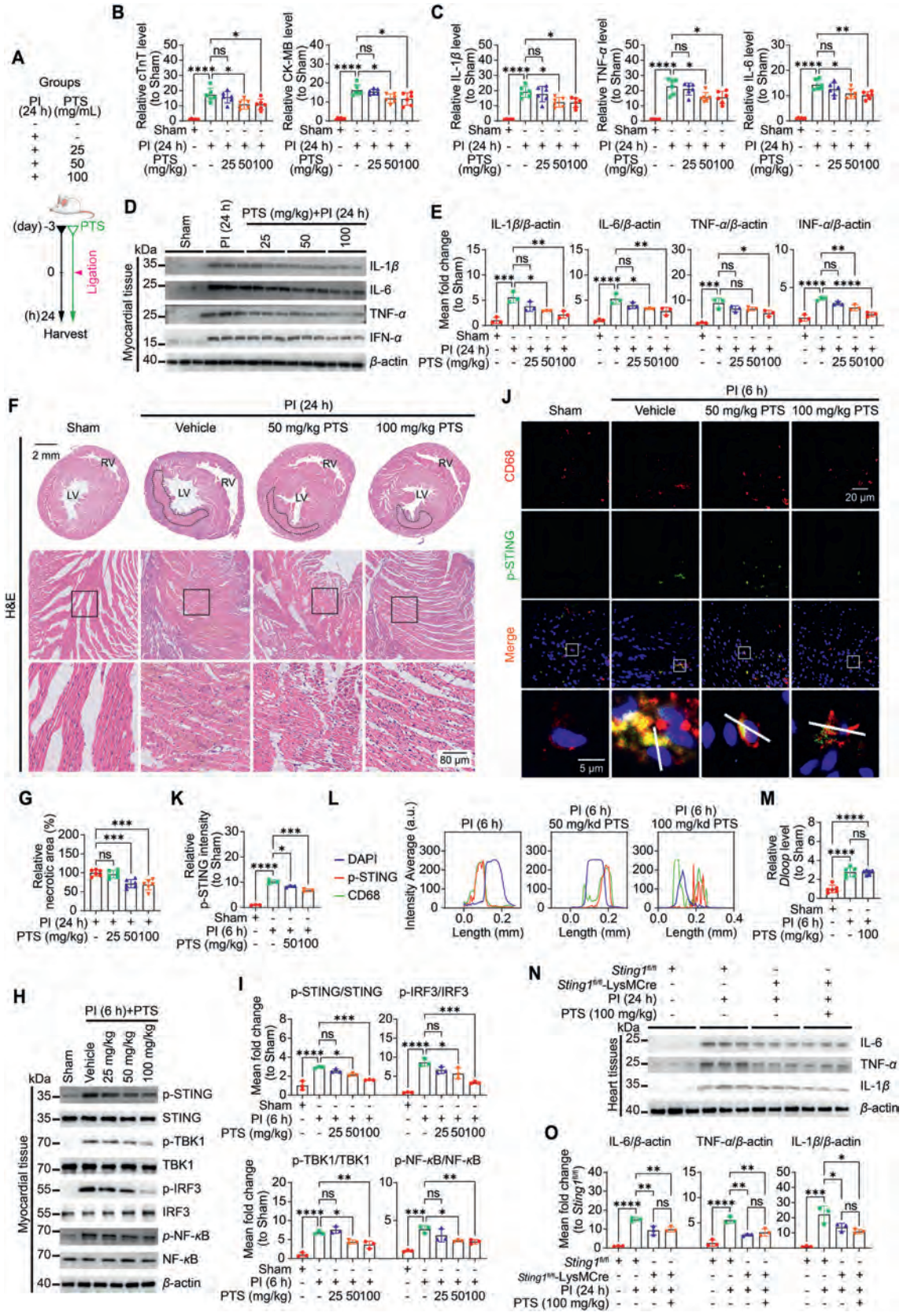

Figure 5 PTS pretreatment attenuates myocardial inflammation and macrophage activation in AMI model rats. (A) The schematic diagram outlines animal grouping and PTS intervention. Rats were administered different doses (25/50/100 mg/kg) of PTS for 3 days before AMI modeling; samples were collected after 6 or 24 h of modeling. (B) Cardiac troponin T and creatine kinase-MB levels in rat serum were measured using ELISA ($n = 6$). (C) IL-1β, TNF-α, and IL-6 levels in rat serum were detected using ELISA ($n = 6$). (D) The expressions IL-1β, IL-6,

ARG-220, TYR-167, and ASN-211 (Fig. 4A). SPR analysis confirmed that PTS has a strong binding capacity to STING under natural conditions (Fig. 4B). Next, we experimentally validated the potential binding interaction between PTS and STING. First, we pretreated BMDMs with PTS for 6, 3, or 0 h, followed by cGAMP administration for 3 h to observe STING pathway activation (Fig. 4C). Notably, pretreatment with PTS for 3 and 6 h significantly reduced the phosphorylation levels of STING, TBK1, IRF3, and NF-κB compared with the control group; the 6-h pretreatment showed greater inhibitory effects. In contrast, simultaneous treatment of BMDMs with PTS and cGAMP did not significantly reduce the phosphorylation levels of these proteins (Fig. 4D and E). These results suggest that PTS pretreatment may allow binding to STING, thereby inhibiting its phosphorylation and downstream signaling mediated by cGAMP. To test this hypothesis, we performed a Co-IP assay to determine the binding ability of STING to TBK1 and IRF3. As shown in Fig. 4F and G, PTS pretreatment for 6 h significantly attenuated the binding of STING to TBK1. Similarly, the binding of STING to IRF3 was also inhibited by PTS (Fig. 4H and I). Furthermore, the binding capacity of PTS with STING was systematically investigated *via* the implementation of CETSA. As illustrated in Fig. 4J and K, the treatment with PTS was discernibly effective in safeguarding STING against temperature-mediated proteolysis, as evidenced by a marked resistance to thermal degradation when contrasted with the untreated control sample.

In the following studies, we obtained *Sting1* knockout BMDMs from *Sting1*$^{fl/fl}$-LysMCre mice (Fig. 4L) and found that PTS did not significantly affect the expression of inflammatory factors in activated macrophages lacking *Sting1* (Fig. 4M and N). Similarly, the fibrosis and hypertrophy phenotypes of cardiomyocytes in the co-culture system were not reversed by PTS (Fig. 4O−Q).

Given that the Tyr261 and Thr263 residues of STING serve as the principal binding sites for PTS, we subsequently utilized adenovirus vectors to induce the overexpression of either wild-type *Sting1* or a mutated *Sting1* variant in BMDMs isolated from *Sting1*$^{fl/fl}$-LysMCre mice. The STING protein encoded by this variant features alanine substitutions at the Tyr261 and Thr263 residues. Following adenovirus infection, we evaluated the effect of PTS intervention on the activation of the STING signaling pathway. The results indicate that PTS treatment did not significantly inhibit the activation of the STING signaling pathway in BMDMs carrying the *Sting1* gene mutations (Fig. 4R and S), thereby underscoring the significance of these specific sites in the regulatory role of PTS on the STING signaling pathway.

Taken together, these data suggest that STING is a specific binding site for PTS and that PTS can competitively bind to STING to inhibit downstream inflammatory signaling in macrophages.

3.5. PTS pretreatment attenuates myocardial inflammation and macrophage activation in AMI model rats

Subsequently, we examined the anti-inflammatory properties of PTS in an AMI model. As shown in Fig. 5A, rats were administered different doses of PTS for 3 days before AMI induction and were euthanized 6 or 24 h PI. The administration of 50 and 100 mg/kg PTS substantially reduced the levels of cardiac troponin T and creatine kinase-MB, markers of acute heart damage, in the blood of rats at 24 h PI (Fig. 5B). Moreover, PTS reduced the levels of IL-1β, IL-6, TNF-α, and IFN-α in the blood and heart tissues of AMI rats at 24 h PI (Fig. 5C−E). Pathological analysis revealed that PTS pretreatment reduced the area of cardiac injury at 24 h PI (Fig. 5F and G). Importantly, immunoblotting showed that PTS pretreatment reversed the phosphorylation levels of STING, TBK1, IRF3, and NF-κB in peri-infarct myocardial tissue at 6 h PI (Fig. 5H and I). Co-localization of p-STING and CD68 indicated that PTS pretreatment inhibited STING phosphorylation in macrophages within myocardial tissue at 6 h PI (Fig. 5J−L).

It is crucial to exclude the possibility that PTS might reduce mtDNA release by safeguarding cardiomyocytes. To address this, we conducted an examination of mtDNA expressions within the peri-infarct myocardial tissues of rats in both the AMI model group and the PTS-treated group. The qRT-PCR results demonstrated that there was no significant difference in mtDNA expression between the two groups of rats at 6 h PI (Fig. 5M). These findings suggest that PTS does not appear to mediate its anti-inflammatory effects through a mechanism involving the reduction of mtDNA release. It is also known that apoptosis may play a significant role in the later stages of myocardial infarction. We thus include the evaluation of apoptosis-related markers to determine whether PTS reduces myocardial damage by modulating apoptotic pathways. Our findings indicate that there was no statistically significant difference in the expression of Bax, Bcl2, and Cleaved PARP-1 between the PTS-treated (100 mg/kg) group and the model group at 24 h PI (Supporting Information Fig. S6A and S6B).

We then validated the anti-inflammatory effects of PTS by employing *Sting1*$^{fl/fl}$ and *Sting1*$^{fl/fl}$-LysMCre mice. The data presented in Fig. 5N and O reveal that, in *Sting1*$^{fl/fl}$ mice, the expressions of IL-1β, IL-6, and TNF-α in the peri-infarct myocardial tissues were significantly increased in the PI (24 h) group relative to the sham group. Across the three PI (24 h) groups, the expression of these inflammatory cytokines was notably reduced in both the *Sting1*$^{fl/fl}$-LysMCre group and the *Sting1*$^{fl/fl}$-LysMCre + PTS group compared to the *Sting1*$^{fl/fl}$ group. Importantly, there was no significant difference observed in the expression of IL-1β, TNF-α, and IL-6 between the *Sting1*$^{fl/fl}$-LysMCre group and the *Sting1*$^{fl/fl}$-LysMCre + PTS group. This finding suggests that the knockout of STING specifically in monocyte-macrophage cells nullifies the anti-inflammatory effects

TNF-α and IFN-α in peri-infarct myocardial tissues were detected *via* Western blotting; Gray value quantification and analysis were carried out in (E) using ImageJ ($n = 3$). (F) Representative H&E-stained images of heart sections; myocardial injury area analysis is shown in (G) ($n = 6$). (H, I) p-STING, p-TBK1, p-IRF3, and p-NF-κB levels in rat peri-infarct tissues were detected and quantified using ImageJ at 6 h PI ($n = 3$). (J) Representative IF images of p-STING and CD68 in each group of rats; fluorescence quantification and analysis were conducted in (K, L) using ImageJ ($n = 3$). (M) The *Dloop* levels in rat peri-infarct tissues were detected using qRT-PCR. (N) *Sting1*$^{fl/fl}$ or *Sting1*$^{fl/fl}$-LysMCre mice were treated with PTS (100 mg/kg) for 3 days then subject to AMI for 24 h. IL-6, TNF-α, and IL-1β levels were detected *via* Western blotting; gray value quantification was performed in (O) using ImageJ ($n = 3$). Data are presented as mean ± SD. $^*P < 0.05$, $^{**}P < 0.01$, $^{***}P < 0.001$, $^{****}P < 0.0001$ (ns, no significance). *P* values were calculated based on one-way ANOVA. cTnT, Cardiac troponin T; CK-MB creatine kinase-MB.

of PTS, indicating a targeted role for STING in the modulatory effects of PTS on inflammation.

3.6. PTS pretreatment attenuates heart failure and myocardial fibrosis in AMI model rats

Finally, we investigated the effects of PTS on AMI-induced heart failure and myocardial fibrosis *in vivo*. Rats were administered PTS prophylactically for 3 days prior to AMI induction, followed by continuous PTS administration for an additional 3 days until treatment termination (Fig. 6A). Cardiac function was assessed by ultrasonography on day 30 PI. PTS pretreatment improved cardiac function, including reversal of the left ventricular internal dimensions during systole and diastole, fractional shortening, and ejection fraction (Fig. 6B and C). H&E and Masson's trichrome staining showed that PTS pretreatment reduced the left ventricular scar area and fibrosis (Fig. 6D−G). Wheat germ agglutinin staining indicated that PTS alleviated AMI-induced myocardial hypertrophy (Fig. 6H and I). Finally, we examined extracellular matrix deposition and myofibroblast activation, which revealed that PTS pretreatment decreased Col I and α-smooth muscle actin expression in a dose-dependent manner (Fig. 6J and K).

Furthermore, considering the prior studies indicating that PTS can stimulate angiogenesis post-ischemia, a critical phenomenon associated with AMI, we investigated the potential effects of prophylactic PTS administration on angiogenesis in rats. Through immunohistochemical analysis, we assessed the expression of CD31, a vascular endothelial cell marker, at the margins of the infarcted myocardial tissue in rats with heart failure. Our results showed no significant difference in vascular density between the PTS-treated group and the model group (Supporting Information Fig. S7A and S7B). This suggests that PTS treatment did not enhance PI angiogenesis. The discrepancy with the findings of previous studies could possibly be due to the relatively short duration of PTS treatment in our study.

4. Discussion

Following AMI, ischemic injury to cardiac tissue initiates a complex interplay of multiple innate and adaptive immune cells in the early inflammatory response. The onset of myocardial ischemia post-AMI leads to cellular damage, cardiomyocyte necrosis, and apoptosis. The onset of myocardial ischemia post-AMI leads to cellular damage, cardiomyocyte necrosis, and apoptosis. This, in turn, triggers a rapid proinflammatory response through a synergistic activation of various processes, such as the complement cascade system, ROS production, and the binding of DAMPs to PRRs. DAMPs, upon adhering to PRRs, notably TLRs and the pivotal NLRP3 inflammasome within the cytosolic protein family, elicit the secretion of potent pro-inflammatory mediators, including cytokines and chemokines[38]. This secretion not only draws inflammatory cells to the affected infarcted area but also amplifies the pro-inflammatory response, significantly heightening the inflammatory load in the aftermath of AMI.

Sterile inflammation following AMI significantly worsens heart injury, and mtDNA, a key DAMP released after cell death, has been reported to activate the immune system as an antigen. However, the role of mtDNA in macrophage recognition and its contribution to the exacerbation of myocardial injury in AMI has not been fully explored. This study demonstrates how mtDNA released from damaged heart tissue triggers an inflammatory response in macrophages in unaffected areas, thereby worsening heart injury. Our *in vivo* and *in vitro* studies further revealed that PTS targets STING to limit inflammatory signaling in macrophages, reducing cardiomyocyte fibrosis and hypertrophy. These findings provide compelling support for the clinical use of PTS in the treatment of AMI and its resulting heart failure.

Cardiac healing after AMI involves multiple phases: an initial inflammatory phase within the first 72 h, a reparative and proliferative phase around Days 7−10, and a final maturation phase. The heart contains resident macrophages, comprising approximately 7%−8% of non-cardiac cells, which can multiply slightly to maintain their roles under normal conditions[5]. However, these resident macrophages are quickly depleted after heart injury; in contrast, circulating monocytes are rapidly recruited to the injury site, where they differentiate into macrophages to manage the inflammatory process. There is evidence that within 30 min of AMI, monocytes are mobilized and infiltrated heart tissue, initially from the circulating blood pool and later from the spleen reservoir, mediated by angiotensin II type 1a receptor signaling[39]. Crucially, new findings suggest that these infiltrating monocytes contribute to neutrophil recruitment, which is a major factor involved in the adverse outcomes of AMI.

Upon tissue entry, monocytes differentiate into dendritic cells and macrophages. Macrophages, which are phenotypically distinct from monocytes, show increased expression of CD68, MHCII, and F4/80 in mice[40]. Macrophages have a dual role in inflammation resolution; their primary function is the clearance of dead tissue from injured heart muscle. However, excessive macrophage activation is associated with myocardial injury. Studies have shown that elevated levels of classical monocytes are linked to reduced left ventricular function 6 months after AMI.

To fully understand the role of macrophages, it is essential to examine their functions in different regions of the heart muscle post-injury. However, much of the research on macrophages following AMI does not differentiate between distinct myocardial regions, such as the infarcted, peri-infarcted, and remote areas. Our data suggests that macrophages accumulate in the necrotic myocardium, as well as the vicinity of the infarcted region. For example, unlike the ischemic region, pro-inflammatory macrophages and Ly-6C^{high} monocytes remain in non-ischemic heart tissue[41]. Similarly, we observed large accumulations of macrophages in the peri-infarct area within 24 h after infarction, as shown by IHC staining (Fig. 1). Researchers have determined that macrophage functions can vary post-AMI depending on their location, which constitutes a significant conceptual shift that could enhance our understanding of macrophage contribution to ventricular remodeling. However, this study did not characterize the specific macrophage subpopulations affected by PTS; these subpopulations should be identified in future research.

Heart inflammation plays a crucial role in cardiac remodeling and the underlying mechanisms of AMI. Elevated concentrations of inflammatory cytokines such as TNF-α and IL-6 are associated with poor outcomes in individuals with AMI[42]. Numerous animal studies have shown that inflammation contributes to heart dysfunction and the development of heart failure. Recent research indicates that the use of IL-1β inhibitors or colchicine as anti-inflammatory treatments may benefit individuals with ischemic heart disease[43,44]. Therefore, it is vital to understand the regulatory mechanisms of heart inflammation and identify new therapeutic targets. Recently, non-infectious inflammation triggered by DAMPs has been recognized as critical in heart-related conditions. Among various DAMPs, mtDNA plays a crucial role in triggering

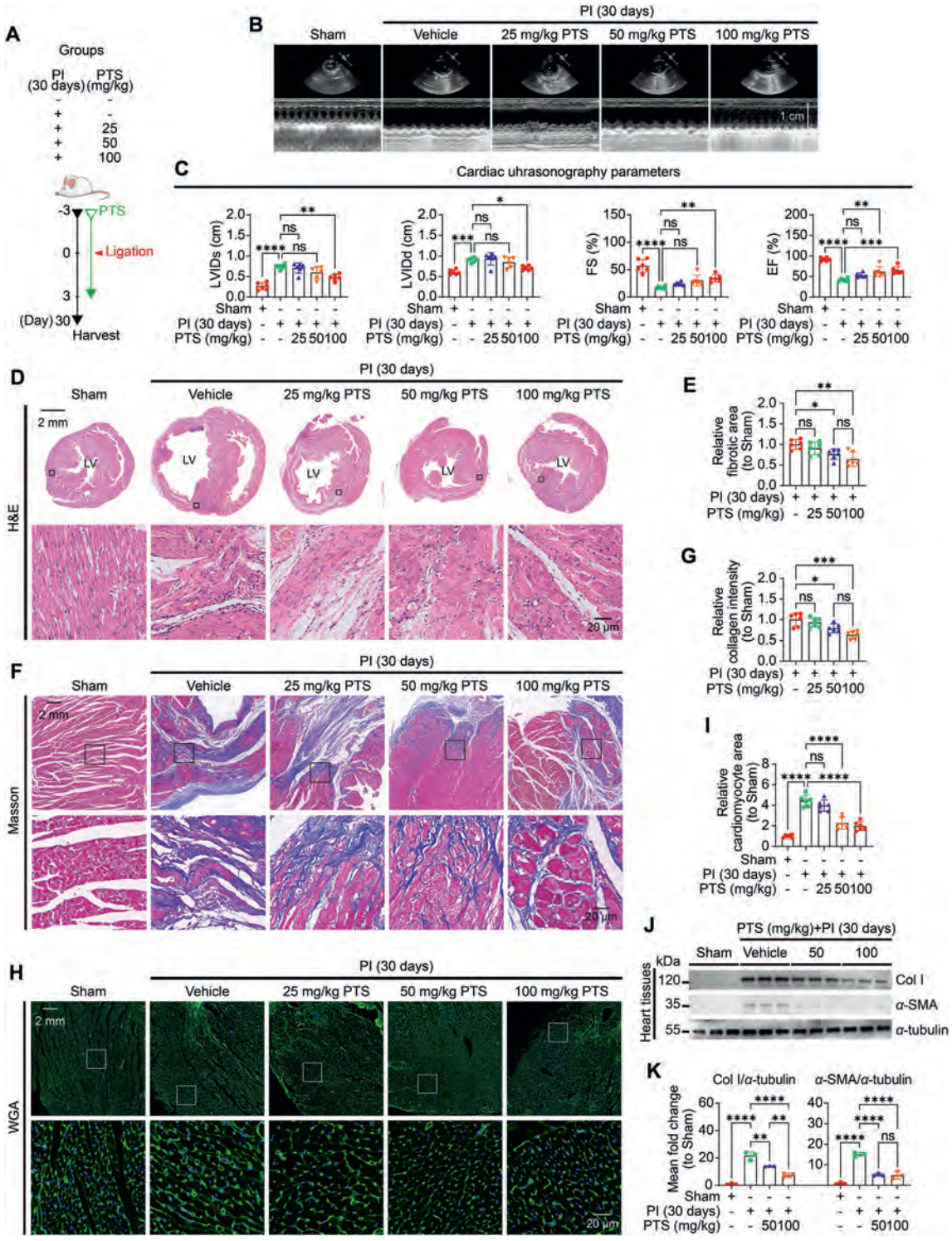

Figure 6 PTS pretreatment attenuates heart failure and myocardial fibrosis in AMI model rats. (A) The schematic diagram outlines animal grouping and PTS intervention. Rats were given different doses (25/50/100 mg/kg) of PTS for 3 days before AMI modeling and continued PTS treatment daily for 3 days. Samples were collected after cardiac ultrasound on the 30th day. (B) Representative images of cardiac ultrasound results in each group; (C) with parameters including left ventricular internal dimensions during systole and diastole, fractional shortening, and ejection fraction ($n = 6$). (D) Representative H&E-stained images of rat heart sections; myocardial scar area quantification is presented in (E) ($n = 6$). (F) Representative images of Masson's trichrome staining of heart sections; collagen fiber content quantification and statistical analysis are shown in (G) ($n = 6$). (H) Representative images of wheat germ agglutinin staining of rat heart sections; mean cross-sectional area analysis of cardiomyocytes is depicted in (I) ($n = 6$). (J) Col I and α-smooth muscle actin levels in rat myocardial tissues were detected *via* Western blotting and quantified in (K) using ImageJ ($n = 3$). Data are presented as mean ± SD. $^{*}P < 0.05$, $^{**}P < 0.01$, $^{***}P < 0.001$, $^{****}P < 0.0001$ (ns, no significance). *P* values were calculated based on one-way ANOVA. LVIDs, left ventricular internal dimensions during systole; LVIDd, left ventricular internal dimensions during diastole; FS, fractional shortening; EF, ejection fraction; WGA, wheat germ agglutinin. α-SMA, α-smooth muscle actin.

heart inflammation during AMI[14]. Specifically, mtDNA that escapes degradation by autophagy activates the cGAS/STING pathways, leading to heart inflammation and dysfunction. Thus, methods that target the mechanisms of mtDNA detection and processing could be a promising therapeutic strategy for AMI. cGAS is a cytoplasmic pattern recognition receptor that detects mtDNA and initiates inflammation by activating cGAS in various cell types, including macrophages. The present study revealed an elevation in mtDNA, rather than nuclear DNA, within infarcted heart tissue, which was linked to the activation of STING pathways and an increase in inflammatory cytokines (Fig. 1).

Several studies have demonstrated the strong association between STING signaling and the macrophage inflammatory response in AMI. Reports indicate that double-stranded DNA from dead heart cells during myocardial infarction activates the cGAS−STING−IRF3 signaling pathway in BMDMs, which may subsequently trigger apoptosis of intact cardiomyocytes. In one study, the use of H-151, a specific inhibitor of the cGAS−STING−IRF3 signaling pathway, reduced macrophage-induced cardiomyocyte apoptosis[45]. Our results are consistent with these findings: we observed that the co-culture of mtDNA-transfected macrophages with cardiomyocytes led to a hypertrophic and fibrotic phenotype in cardiomyocytes (Fig. 2). This phenotype may be related to the induced expression of renin and angiotensinogen-converting enzyme in macrophages, leading to the production of angiotensin II through autocrine effects[46]. Notably, a recent study showed that STING protein levels are elevated in infarcted heart tissue, and STING blockade resulted in a significant reduction in cardiac fibrosis 2 weeks post−MI[47]. Additionally, hypoxia-induced death of cardiomyocytes and fibroblasts led to increased STING expression in macrophages. However, these results slightly differ from our findings; we observed elevated levels of phosphorylated STING, but not total STING protein, in the peri-infarct area early after infarction (6 h). This difference may be related to the timing of infarction and the specific sites tested.

Research on targeting macrophage STING as a therapy for AMI is limited. In this study, mononuclear macrophage system-specific STING knockout mice exhibited more favorable cardioprotective effects in AMI, as evidenced by a smaller area of myocardial injury and lower expression of inflammatory factors, suggesting that targeting macrophage STING could be a potential therapeutic strategy for AMI (Fig. 1). *In vitro*, PTS effectively inhibited STING activity, as demonstrated by the suppression of mtDNA-induced macrophage STING pathway activation. Remarkably, in the co-culture system, PTS attenuated the induction of cardiomyocyte hypertrophic and fibrotic phenotypes by activated macrophages (Fig. 3). Based on the potential regulatory role of PTS on STING, we used molecular docking techniques to determine the potential binding capacity of PTS to STING, which was experimentally validated through SPR (Fig. 4). *In vivo*, PTS reduced heart tissue damage and inflammation during the early phase of AMI in model rats; it also decreased myocardial fibrosis and heart failure during the later phase of AMI. However, considering the previously reported cardioprotective effects of PTS, further studies using *Sting1*$^{fl/fl}$-LysMCre mice are needed to confirm the efficacy of PTS in the AMI model.

Building upon the foundation of previous research on PTS, this study not only validates existing findings but also introduces new perspectives for investigating the cardioprotective effects of PTS. Prior *in vitro* and *in vivo* studies have explored PTS's antioxidant properties in the context of acute ischemic cardiomyopathy. These findings reveal that PTS protects cardiac fibroblasts by boosting nuclear factor erythroid 2-related factor 2 expression *via* the fine-tuning of Kelch-like ECH-associated protein 1 activity. This action stimulates the production of downstream antioxidant molecules, which in turn alleviate mitochondrial membrane damage caused by ROS. Moreover, the pivotal role of macrophages in ROS generation during acute inflammatory injury is well established. The capacity of PTS to modulate ROS levels in macrophages, however, has yet to be elucidated. To address this gap, a comprehensive investigation into the mechanisms by which PTS may regulate macrophage oxidative stress and contribute to myocardial protection is imperative. Such an exploration would enhance our understanding of PTS's multifaceted mechanisms of action, particularly its potential to shield against mitochondrial-related pathologies.

5. Conclusions

During the initial phase of AMI, the activation of macrophage STING signaling by mtDNA in areas not directly affected by the infarction exacerbates heart damage. PTS improves myocardial fibrosis and heart failure in AMI model mice by binding to macrophage STING, thereby interfering with inflammatory signaling and inhibiting the development of myocardial fibrosis and hypertrophic phenotypes.

Acknowledgments

This work was supported by the National Natural Science Foundation of China (Grant Number: 8217153243).

Author contributions

Conceptualization: Yongxiang Gao; Methodology: Huan Yao; Formal analysis: Qingman He; Investigation: Huan Yao, Qingman He, Shujun Wei, Li Xiang; Data curation: Yuanyuan Luo, Cong Huang; Writing − original draft: Huan Yao; Writing − review & editing: Yongxiang Gao; Visualization: Weiwei Liu; Supervision: Chuan Zheng; Project administration: Yongxiang Gao, Xueping Li; Funding acquisition: Xueping Li. Huan Yao and Qingman He are contributed equally to this work.

Conflicts of interest

The authors declare no conflicts of interest.

Appendix A. Supporting information

Supporting information to this article can be found online at https://doi.org/10.1016/j.apsb.2025.06.014.

References

1. Cung TT, Morel O, Cayla G, Rioufol G, Garcia-Dorado D, Angoulvant D, et al. Cyclosporine before PCI in patients with acute myocardial infarction. *N Engl J Med* 2015;**373**:1021−31.
2. Ong SB, Hernández-Reséndiz S, Crespo-Avilan GE, Mukhametshina RT, Kwek XY, Cabrera-Fuentes HA, et al. Inflammation following acute myocardial infarction: multiple players, dynamic roles, and novel therapeutic opportunities. *Pharmacol Ther* 2018;**186**:73−87.

3. Barrère-Lemaire S, Vincent A, Jorgensen C, Piot C, Nargeot J, Djouad F. Mesenchymal stromal cells for improvement of cardiac function following acute myocardial infarction: a matter of timing. *Physiol Rev* 2024;**104**:659−725.
4. Berezin AE, Berezin AA. Adverse cardiac remodelling after acute myocardial infarction: old and new biomarkers. *Dis Markers* 2020; **2020**:1215802.
5. Kologrivova I, Shtatolkina M, Suslova T, Ryabov V. Cells of the immune system in cardiac remodeling: main players in resolution of inflammation and repair after myocardial infarction. *Front Immunol* 2021;**12**:664457.
6. Longnus SL, Rutishauser N, Gillespie MN, Reichlin T, Carrel TP, Sanz MN. Mitochondrial damage-associated molecular patterns as potential biomarkers in DCD heart transplantation: lessons from myocardial infarction and cardiac arrest. *Transplant Direct* 2022;**8**: e1265.
7. Mauro AG, Bonaventura A, Mezzaroma E, Quader M, Toldo S. NLRP3 inflammasome in acute myocardial infarction. *J Cardiovasc Pharmacol* 2019;**74**:175−87.
8. Oka T, Hikoso S, Yamaguchi O, Taneike M, Takeda T, Tamai T, et al. Mitochondrial DNA that escapes from autophagy causes inflammation and heart failure. *Nature* 2012;**485**:251−5.
9. Fujiwara Y, Kikuchi H, Aizawa S, Furuta A, Hatanaka Y, Konya C, et al. Direct uptake and degradation of DNA by lysosomes. *Autophagy* 2013;**9**:1167−71.
10. Sasai M, Linehan MM, Iwasaki A. Bifurcation of Toll-like receptor 9 signaling by adaptor protein 3. *Science* 2010;**329**:1530−4.
11. Broz P, Dixit VM. Inflammasomes: mechanism of assembly, regulation and signalling. *Nat Rev Immunol* 2016;**16**:407−20.
12. Deswal A, Petersen NJ, Feldman AM, Young JB, White BG, Mann DL. Cytokines and cytokine receptors in advanced heart failure: an analysis of the cytokine database from the Vesnarinone trial (VEST). *Circulation* 2001;**103**:2055−9.
13. Markousis-Mavrogenis G, Tromp J, Ouwerkerk W, Devalaraja M, Anker SD, Cleland JG, et al. The clinical significance of interleukin-6 in heart failure: results from the BIOSTAT-CHF study. *Eur J Heart Fail* 2019;**21**:965−73.
14. Enzan N, Matsushima S, Ikeda S, Okabe K, Ishikita A, Yamamoto T, et al. ZBP1 protects against mtDNA-induced myocardial inflammation in failing hearts. *Circ Res* 2023;**132**:1110−26.
15. Zhong Z, Liang S, Sanchez-Lopez E, He F, Shalapour S, Lin XJ, et al. New mitochondrial DNA synthesis enables NLRP3 inflammasome activation. *Nature* 2018;**560**:198−203.
16. Decout A, Katz JD, Venkatraman S, Ablasser A. The cGAS−STING pathway as a therapeutic target in inflammatory diseases. *Nat Rev Immunol* 2021;**21**:548−69.
17. Natarajan N, Florentin J, Johny E, Xiao H, O'Neil SP, Lei L, et al. Aberrant mitochondrial DNA synthesis in macrophages exacerbates inflammation and atherosclerosis. *Nat Commun* 2024;**15**:7337.
18. Sun SJ, Jiao XD, Chen ZG, Cao Q, Zhu JH, Shen QR, et al. Gasdermin-E-mediated pyroptosis drives immune checkpoint inhibitor-associated myocarditis *via* cGAS−STING activation. *Nat Commun* 2024;**15**:6640.
19. Guo Y, You Y, Shang FF, Wang X, Huang B, Zhao B, et al. iNOS aggravates pressure overload-induced cardiac dysfunction *via* activation of the cytosolic-mtDNA-mediated cGAS−STING pathway. *Theranostics* 2023;**13**:4229−46.
20. Lei Y, VanPortfliet JJ, Chen YF, Bryant JD, Li Y, Fails D, et al. Cooperative sensing of mitochondrial DNA by ZBP1 and cGAS promotes cardiotoxicity. *Cell* 2023;**186**:3013−32.
21. Luo W, Zou X, Wang Y, Dong Z, Weng X, Pei Z, et al. Critical role of the cGAS−STING pathway in doxorubicin-induced cardiotoxicity. *Circ Res* 2023;**132**:e223−42.
22. Huang Y, Yu J, Wan F, Zhang W, Yang H, Wang L, et al. Panaxatriol saponins attenuated oxygen−glucose deprivation injury in PC12 cells *via* activation of PI3K/Akt and Nrf2 signaling pathway. *Oxid Med Cell Longev* 2014;**2014**:978034.
23. Hui Z, Sha DJ, Wang SL, Li CS, Qian J, Wang JQ, et al. Panaxatriol saponins promotes angiogenesis and enhances cerebral perfusion after ischemic stroke in rats. *BMC Compl Alternative Med* 2017;**17**: 70.
24. Qi H, Huang Y, Yang Y, Dou G, Wan F, Zhang W, et al. Anti-platelet activity of panaxatriol saponins is mediated by suppression of intracellular calcium mobilization and ERK2/p38 activation. *BMC Compl Alternative Med* 2016;**16**:174.
25. Yao H, He Q, Huang C, Wei S, Gong Y, Li X, et al. Panaxatriol saponin ameliorates myocardial infarction-induced cardiac fibrosis by targeting Keap1/Nrf2 to regulate oxidative stress and inhibit cardiac-fibroblast activation and proliferation. *Free Radic Biol Med* 2022; **190**:264−75.
26. Yao H, Xie Q, He Q, Zeng L, Long J, Gong Y, et al. Pretreatment with panaxatriol saponin attenuates mitochondrial apoptosis and oxidative stress to facilitate treatment of myocardial ischemia-reperfusion injury *via* the regulation of Keap1/Nrf2 activity. *Oxid Med Cell Longev* 2022; **2022**:9626703.
27. Luo M, Yan D, Sun Q, Tao J, Xu L, Sun H, et al. Ginsenoside Rg1 attenuates cardiomyocyte apoptosis and inflammation *via* the TLR4/NF-κB/NLRP3 pathway. *J Cell Biochem* 2020;**121**:2994−3004.
28. Lee IA, Hyam SR, Jang SE, Han MJ, Kim DH. Ginsenoside Re ameliorates inflammation by inhibiting the binding of lipopolysaccharide to TLR4 on macrophages. *J Agric Food Chem* 2012;**60**:9595−602.
29. Zhang S, Chen Q, Jin M, Ren J, Sun X, Zhang Z, et al. Notoginsenoside R1 alleviates cerebral ischemia/reperfusion injury by inhibiting the TLR4/MyD88/NF-κB signaling pathway through microbiota−gut−brain axis. *Phytomedicine* 2024;**128**:155530.
30. Li C, Fan C, Zhao J, Di M, Sui C, Han L, et al. Panaxatriol saponins promote M2 polarization of BV2 cells to reduce inflammation and apoptosis after glucose/oxygen deprivation by activating STAT3. *Inflammation* 2020;**43**:2109−18.
31. Wu Y, Yin X, Wijaya C, Huang MH, McConnell BK. Acute myocardial infarction in rats. *J Vis Exp* 2011;**16**:2464.
32. Li X, Xu G, Wei S, Zhang B, Yao H, Chen Y, et al. Lingguizhugan decoction attenuates doxorubicin-induced heart failure in rats by improving TT-SR microstructural remodeling. *BMC Compl Alternative Med* 2019;**19**:360.
33. Yao H, Wei S, Xiang Y, Wu Z, Liu W, Wang B, et al. Kangfuxin oral liquid attenuates bleomycin-induced pulmonary fibrosis *via* the TGF-β1/Smad pathway. *Evid Based Complement Alternat Med* 2019;**2019**: 5124026.
34. Mendoza R, Banerjee I, Manna D, Reghupaty SC, Yetirajam R, Sarkar D. Mouse bone marrow cell isolation and macrophage differentiation. *Methods Mol Biol* 2022;**2455**:85−91.
35. Li C, Rong X, Qin J, Wang S. An improved two-step method for extraction and purification of primary cardiomyocytes from neonatal mice. *J Pharmacol Toxicol Methods* 2020;**104**:106887.
36. Jiang L, Yin X, Chen YH, Chen Y, Jiang W, Zheng H, et al. Proteomic analysis reveals ginsenoside Rb1 attenuates myocardial ischemia/reperfusion injury through inhibiting ROS production from mitochondrial complex I. *Theranostics* 2021;**11**:1703−20.
37. Yang A, Zeng K, Huang H, Liu D, Song X, Qian Y, et al. Usenamine A induces apoptosis and autophagic cell death of human hepatoma cells *via* interference with the Myosin-9/actin-dependent cytoskeleton remodeling. *Phytomedicine* 2023;**116**:154895.
38. Arslan F, de Kleijn DP, Pasterkamp G. Innate immune signaling in cardiac ischemia. *Nat Rev Cardiol* 2011;**8**:292−300.
39. Dutta P, Nahrendorf M. Monocytes in myocardial infarction. *Arterioscler Thromb Vasc Biol* 2015;**35**:1066−70.
40. Peet C, Ivetic A, Bromage DI, Shah AM. Cardiac monocytes and macrophages after myocardial infarction. *Cardiovasc Res* 2020;**116**:1101−12.
41. Zouggari Y, Ait-Oufella H, Bonnin P, Simon T, Sage AP, Guérin C, et al. B lymphocytes trigger monocyte mobilization and impair heart function after acute myocardial infarction. *Nat Med* 2013;**19**:1273−80.
42. Zhang H, Dhalla NS. The role of pro-inflammatory cytokines in the pathogenesis of cardiovascular disease. *Int J Mol Sci* 2024;**25**:1082.

43. Ridker PM, Everett BM, Thuren T, MacFadyen JG, Chang WH, Ballantyne C, et al. Antiinflammatory therapy with canakinumab for atherosclerotic disease. *N Engl J Med* 2017;**377**:1119−31.
44. Nidorf SM, Fiolet ATL, Mosterd A, Eikelboom JW, Schut A, Opstal TSJ, et al. Colchicine in patients with chronic coronary disease. *N Engl J Med* 2020;**383**:1838−47.
45. Hu S, Gao Y, Gao R, Wang Y, Qu Y, Yang J, et al. The selective STING inhibitor H-151 preserves myocardial function and ameliorates cardiac fibrosis in murine myocardial infarction. *Int Immunopharmacol* 2022;**107**:108658.
46. Weber KT, Sun Y, Bhattacharya SK, Ahokas RA, Gerling IC. Myofibroblast-mediated mechanisms of pathological remodelling of the heart. *Nat Rev Cardiol* 2013;**10**:15−26.
47. Kong W, Chen J, Ruan X, Xu X, Li X, Bao M, et al. Cardiac injury activates STING signaling *via* upregulating SIRT6 in macrophages after myocardial infarction. *Life Sci* 2024;**341**:122474.